GSA Data Repository 2016126

Coseismic extension from surface cracks reopened by the 2014 Pisagua, northern Chile, earthquake sequence

Scott et al.

GPS Methods:

We calculate the daily time series for 12 continuous GPS stations that are part of the Central Andean Tectonic Observatory Geodetic Array (Simons et al., 2010) or an array operated by the Chilean government, and are all processed by Blewitt (2015). From the time series of station positions, we calculate the coseismic displacement during the April 1 M_w8.1 earthquake by subtracting the station position on March 31 from that on April 2, 2014. Likewise the April 3 M_w7.7 coseismic displacements were calculated by subtracting the position on April 2 from the position on April 4, 2014. Unfortunately station CLLA (Figure 1S) had a recording gap during the earthquakes, so the separated coseismic displacements are available for just 11 stations, but CLLA can still be used to calculate the overall strain from the entire sequence, combined. We solve for the distance-weighted infinitesimal displacement gradient tensor (Allmendinger et al., 2009; Cardozo and Allmendinger, 2009) by independently inverting the three sets of GPS displacement vectors. We test a range of distance weighting parameters from 35 to 150 km, and select the one that produces the most consistent fit between the mean crack orientations and the GPS-inferred maximum horizontal shortening axes. We find 50 km to be the optimal distance weighting parameter.

Interferometric Synthetic Aperture Radar (InSAR) Methods:

We generate a coseismic ascending interferogram using X-band SAR imagery with a wavelength of 3.1 cm from the TerraSAR-X satellite shown in Figure DR7. We process the

interferogram with precise scientific orbits (Yoon et al., 2009) using the Repeat Orbit Interferometry PACkage (ROI_PAC) produced by Rosen et al. (2004). We remove the topographic phase using a 90 m digital elevation model (DEM) from the Shuttle Radar Topography Mission (SRTM, Farr et al., 2007).

InSAR Analysis:

We use InSAR data to characterize potential gradients in the displacement field over spatial scales that are too short to be well-sampled by the GPS data. We produce maps of the SAR displacement field at a spatial resolution of 30 m. This is a sufficient spatial resolution to detect if the large crack openings measured in the field are indicative of anomalous strain concentrated within the crack transects. The satellite line-of-sight direction oriented at 29° from vertical results in a combined sensitivity to horizontal and vertical deformation.

The interferogram shows no strain concentrated over the Pisagua transect (Figure DR8a). We dismiss atmospheric effects as a noise source that could significantly contaminate the strain signal over the transect. Atmospheric artifacts in InSAR data are largely caused by differences in humidity at the timing of the SAR acquisitions and result in spatially coherent noise signals that approximately scale with elevation. Because elevation is relatively smooth over the transect length (Figure DR8b), atmospheric noise is unlikely to have significantly contaminated the InSAR signal.

The summed crack apertures of 10.5 cm measured in the field at the Pisagua transect project to ~5 cm of displacement in the SAR line-of-sight. Had the cracks concentrated this amount of deformation, we would expect to see almost two fringes of displacement localized to the ~1 km transect (Figure DR8c & DR8d). The fact that the interferometric phase is not

disrupted across the cracked area suggests that the cracks do not accommodate enhanced coseismic strain relative to the immediately surrounding areas.

Topographic control on crack orientations

Cracks commonly form along or near topographic scarps with opening vectors aligned with the direction of maximum relief even when the orientation is poorly aligned with the static strain field. This suggests that the focusing of seismic waves across underlying faults and local gravitational instabilities influence crack formation and orientation.

We assess the dominant trends of topographic scarps over the rupture area from a slope map (Figure DR5). NS-striking topographic scarps largely outline normal faults and the Coastal Escarpment. Margin perpendicular structures include EW to ENE striking reverse faults and several large canyons. North of the Quebrada de Camarones, fault scarps rotate to a dominant NE orientation (Figure DR5). We separate scarps by azimuth and show a higher than average concentration of scarps with NS and ENE/EW orientations (Figure DR6).

We consider two approaches of accounting for the topographic control in the comparison of the strain axes inferred from the crack orientations and geodetic datasets. In the first, we simply include all mean crack orientations in the comparison calculation (Figure 3a). This approach benefits from including all data, irrespective of any topographic control. In the second, we remove cracks with orientations that deviate by more than 50° from the GPS inferred strain axes for both the M_w8.8 and M_w7.7 earthquakes from our statistical analysis (Figure 3b & 3c). ~75% of the removed field sites lie along or near EW to ENE striking structures.

Transect	Start Lat, Long (°)	End Lat, Long (°)	Start Elev. (m)	End Elev. (m)	Length (m)	Opening (cm)	Date
Pisagua	-19.6934, -70.1336	-19.6908, -70.1253	765	812	915	10.5	July 5, 2014
Caleta Buena	-20.0225, -70.0777	-20.0223, -70.0721	584	600	591	32.4	April 7, 2014
Punta de Lobos 1	-21.0380, -70.1275	-21.0349, -70.1225	629	583	625	3.0	July 8, 2014
Punta de Lobos 2	-21.0404, -70.1272	-21.0400, -70.1223	632	595	511	6.5	July 8, 2014
Punta de Lobos 3	-21.0389, -70.1226	-21.0375, -70.1220	620	590	500	1.0	July 8, 2014

Table DR1: Location of transects.

Transect		Cumulative Opening (cm)	Transect length (m)	Apparent Coseismic Strain	Orientation
Pisagua	Cracks	10.5	915	1.15×10^{-4}	350.9±11.8°
	GPS*	0.19	915	2.07×10^{-6}	354°
Caleta Buena	Cracks	32.4	591	5.48×10^{-4}	019.4±13.7°
	GPS*	0.21	591	3.52×10^{-6}	008.4°
Punta de Lobos	Cracks (average of 3 transects)	3.5	545	6.42×10^{-5}	006.9±9.2°
	Baker et al. (2013) 150 year event	0.39	545	$7.1\pm2.3\times10^{-6}$	N/A
	Baker et al. (2013) 300 year event	0.78	545	$14.2\pm2.3\times10^{-6}$	N/A

*GPS strains are calculated for a 50 km distance-weighting factor.
Punta de Lobos results are an average of the three transects at the particular site.

Table DR2: Summary of strain magnitude and orientation calculations. GPS openings are the strain values multiplied by the transect length. The 150 and 300 year events at Punta de Lobos refer to the expected strain release from great earthquakes with recurrence intervals of 150 and 300 years, respectively. The per event strain magnitudes are inferred from the permanent extension recorded in a suite of cracks within surfaces that date to 0.8-1.1 Ma (Baker et al., 2013).

2016126_Supplemental Data table_mean.xlsx

Supplementary Figures

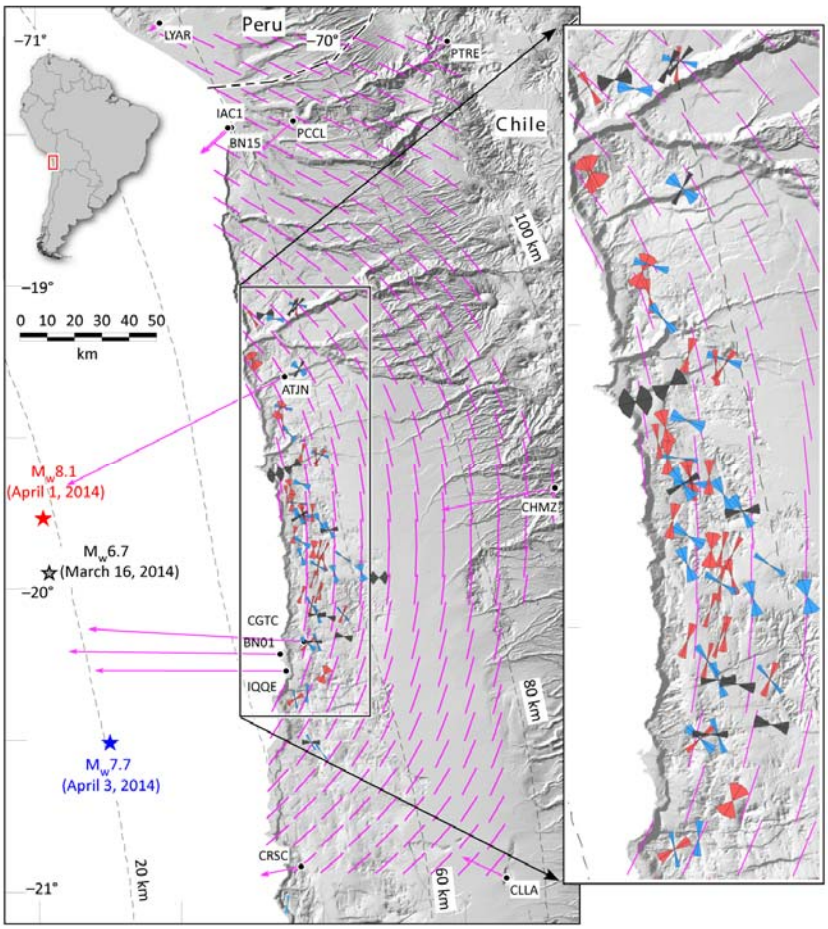

Figure DR1: Location map of northern Chile between latitudes of 18° and 21°S. Stars represent Global Centroid Mean Tensor (GCMT) earthquake locations for the three largest events in the 2014 sequence. Pink arrows indicate GPS displacements extracted from Caltech (Simons et al., 2010) and Chilean government stations as processed by Blewitt (2015) for the entire earthquake sequence. The pink tick marks represent the principal horizontal shortening axes obtained by inverting the GPS data for strain using a 50 km distance weighting constant plotted at a 10 km spacing. Colored "bowties" are the average and 2σ spread of coseismic crack orientations at the 72 sites: red and blue bowties represent cracks most closely aligned with the

M_w8.1 and M_w7.7 strain fields, respectively. Gray bowties represent cracks whose orientation deviates from the GPS inferred strain axes by more than 50°. Dashed white lines are contours of the depth of the subducted plate from the SLAB 1.0 model in 20 km intervals (Hayes et al., 2012).

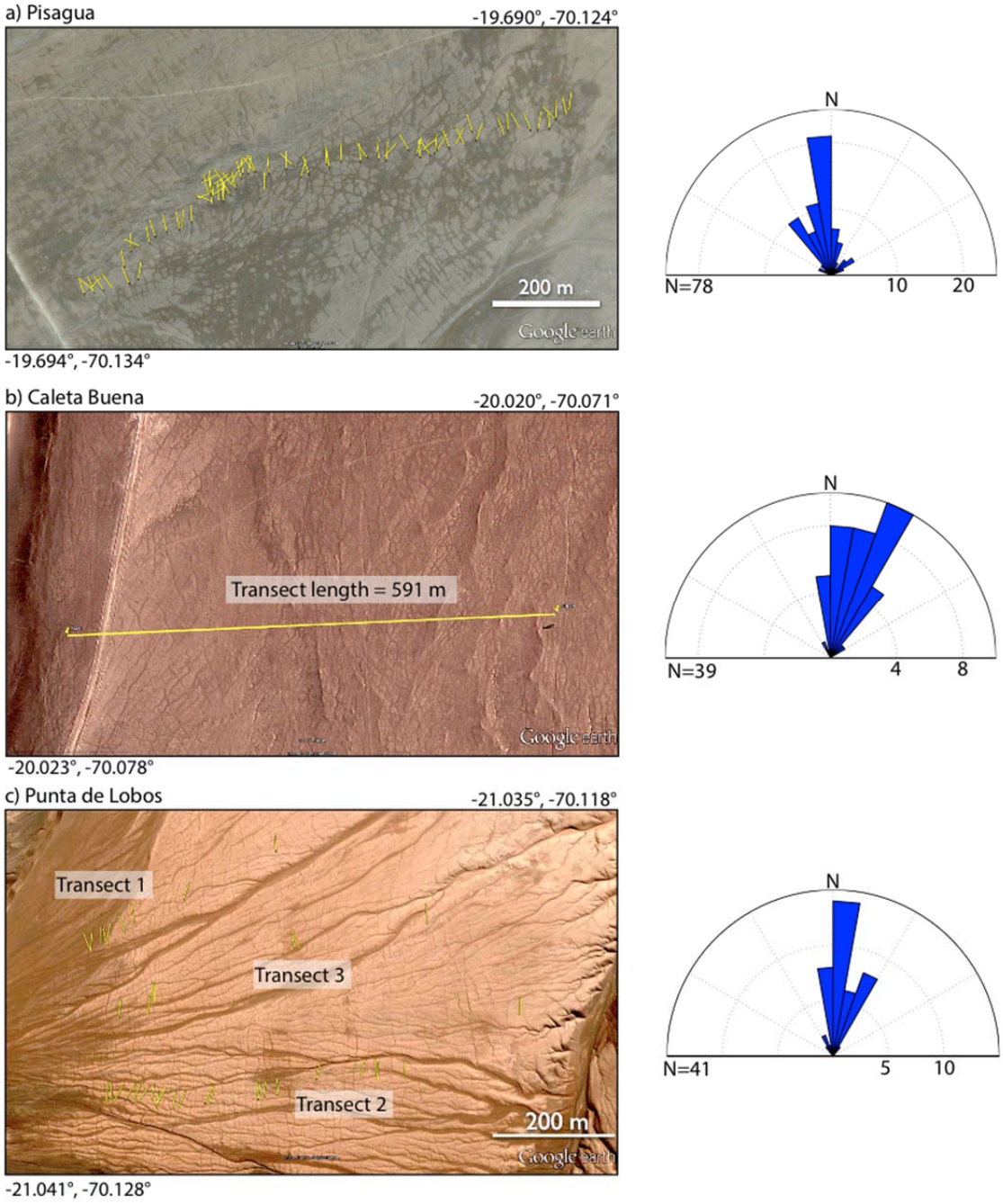

Figures DR2: Google Earth imagery of the measured transects near Pisagua (a), Caleta Buena (b), and Punta de Lobos (c). Yellow lines represent fresh coseismic cracks. Rose diagrams show the fresh crack orientations. At the Caleta Buena site, there are two old crack sets, NNE and NW-striking but, as shown in the rose diagram, only the NNE set was reactivated in 2014.

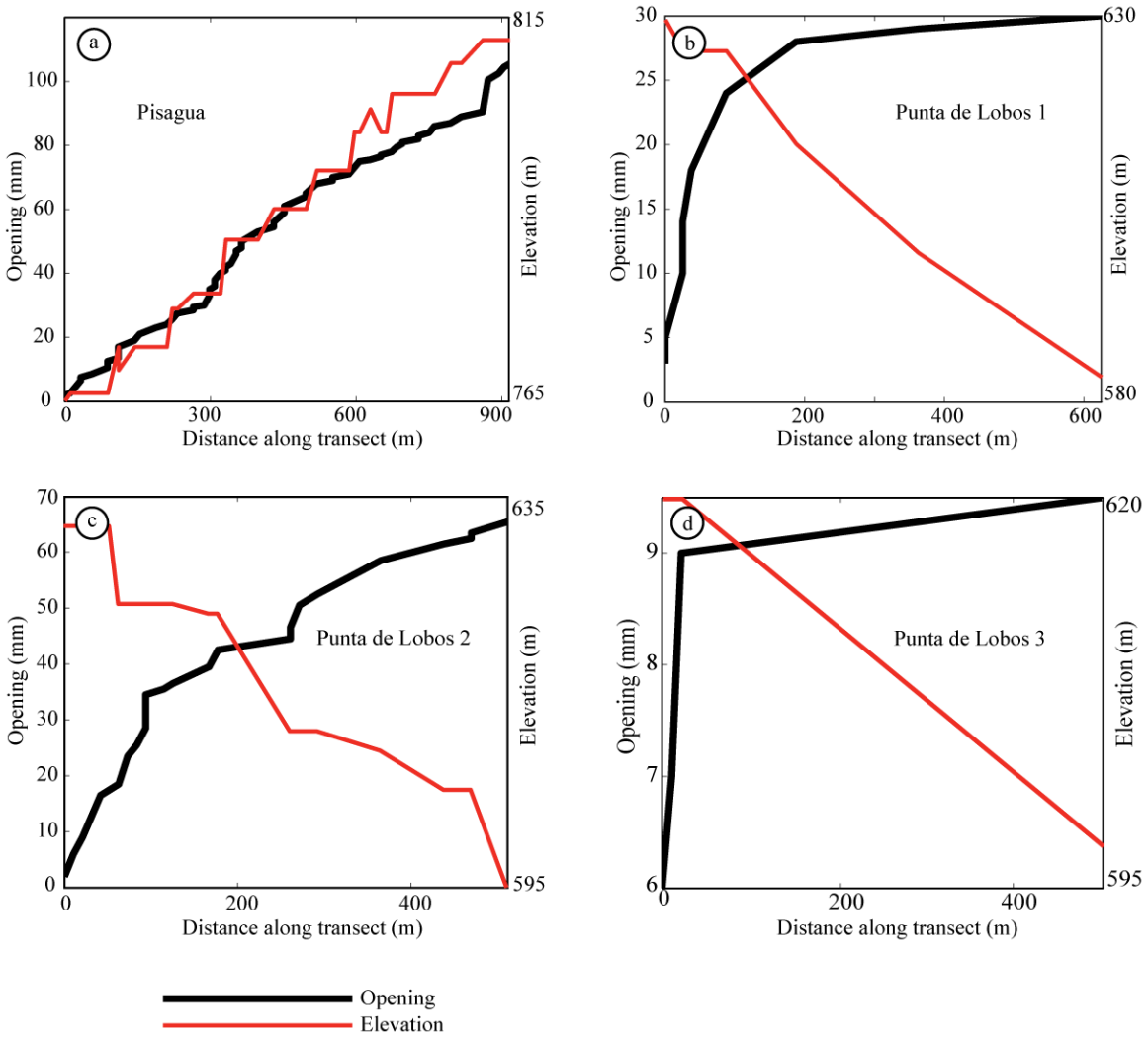

Figure DR3: Opening and elevation vs. distance along transects at the Pisagua and Punta de Lobos sites.

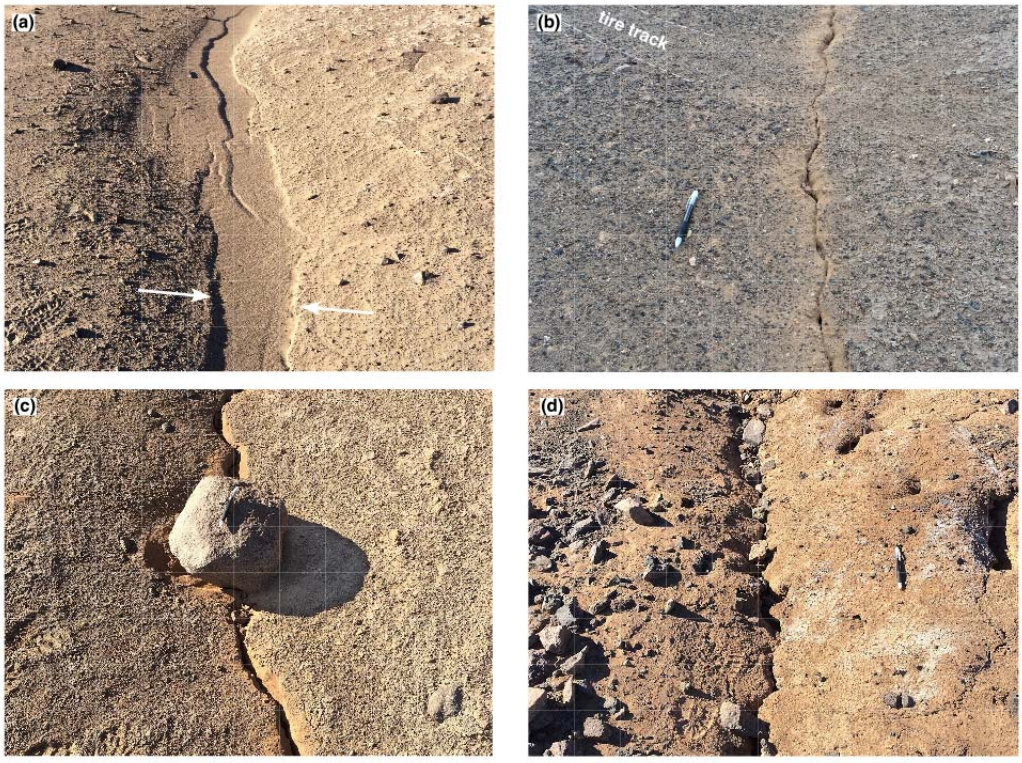

Figure DR4: Color version of Figure 2 in the main text.

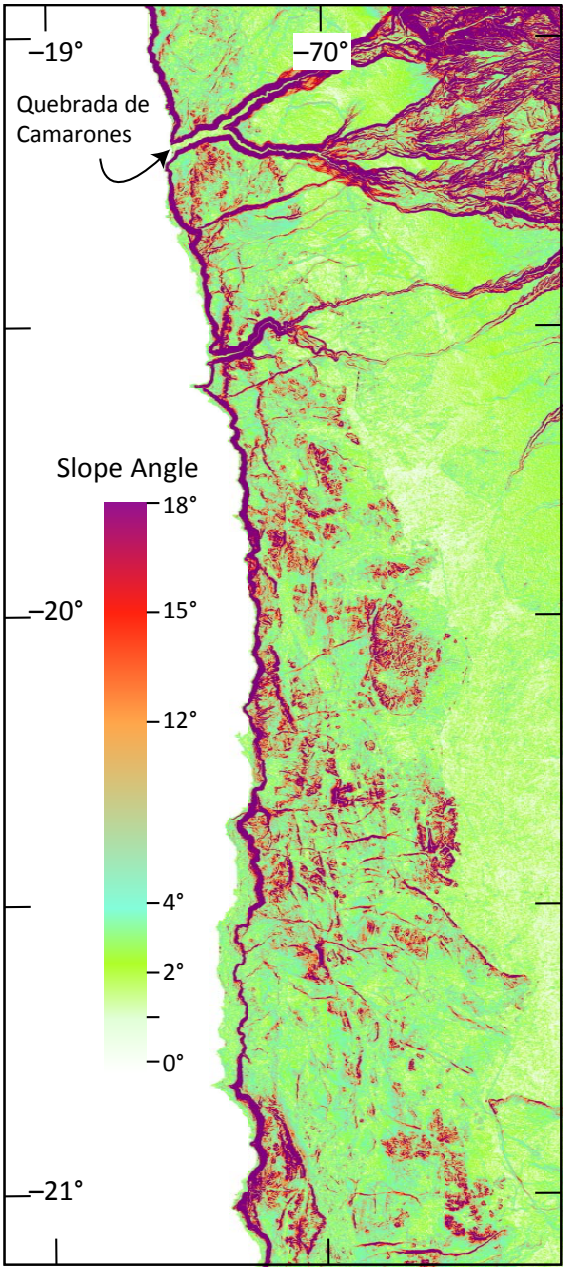

Figure DR5: Map of slope angles in the Coastal Cordillera of northern Chile.

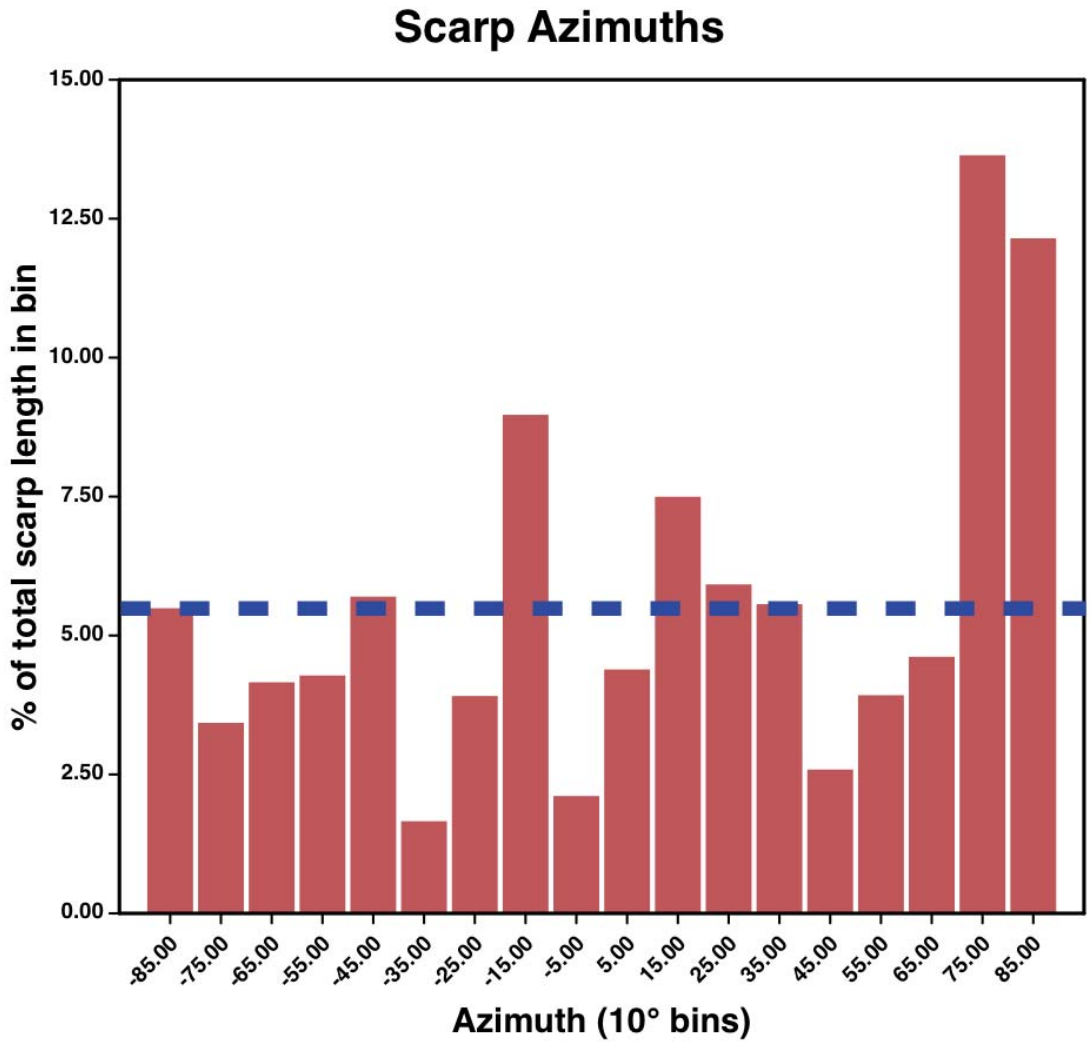

Figure DR6: Percent of total scarp length in 10° azimuthal bins between –90° (270°) and 90° scarp azimuth. The dashed blue line indicates the expected percentage of total scarp length given a uniform distribution of topographic scarps.

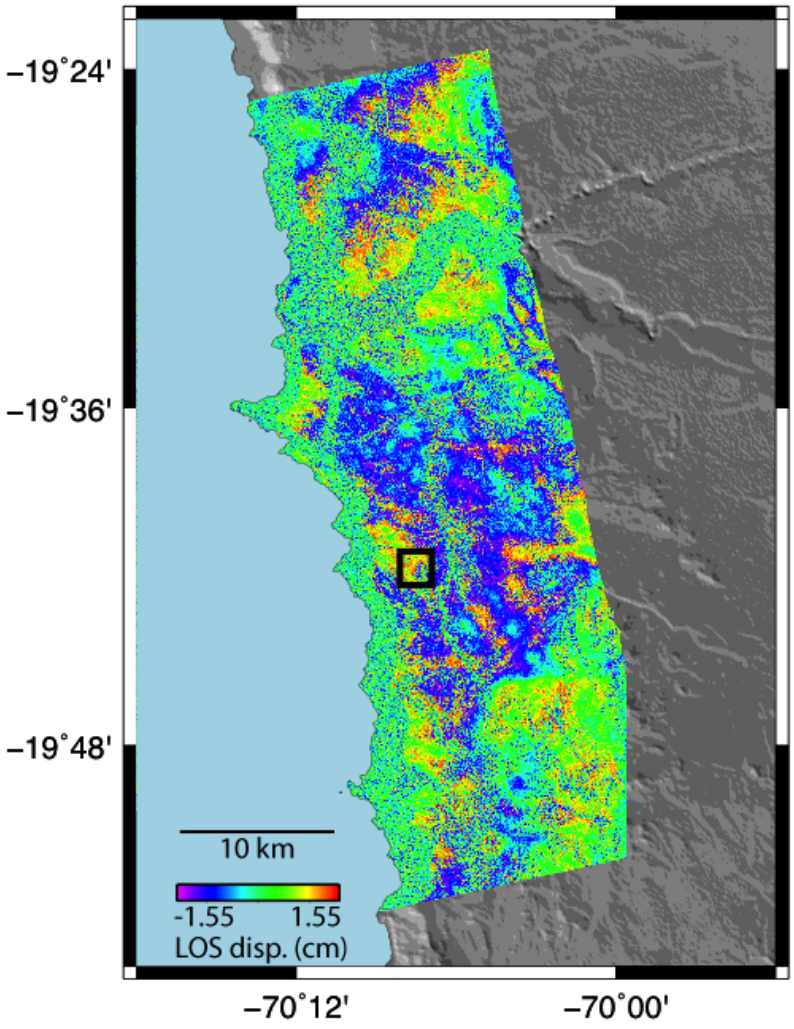

Figure DR7: Coseismic ascending TerraSAR-X imagery. The wrapped, unfiltered interferogram spans December 18, 2011- April 2, 2014. The black box outlines the Pisagua site and the zoomed area in Figure DR8.

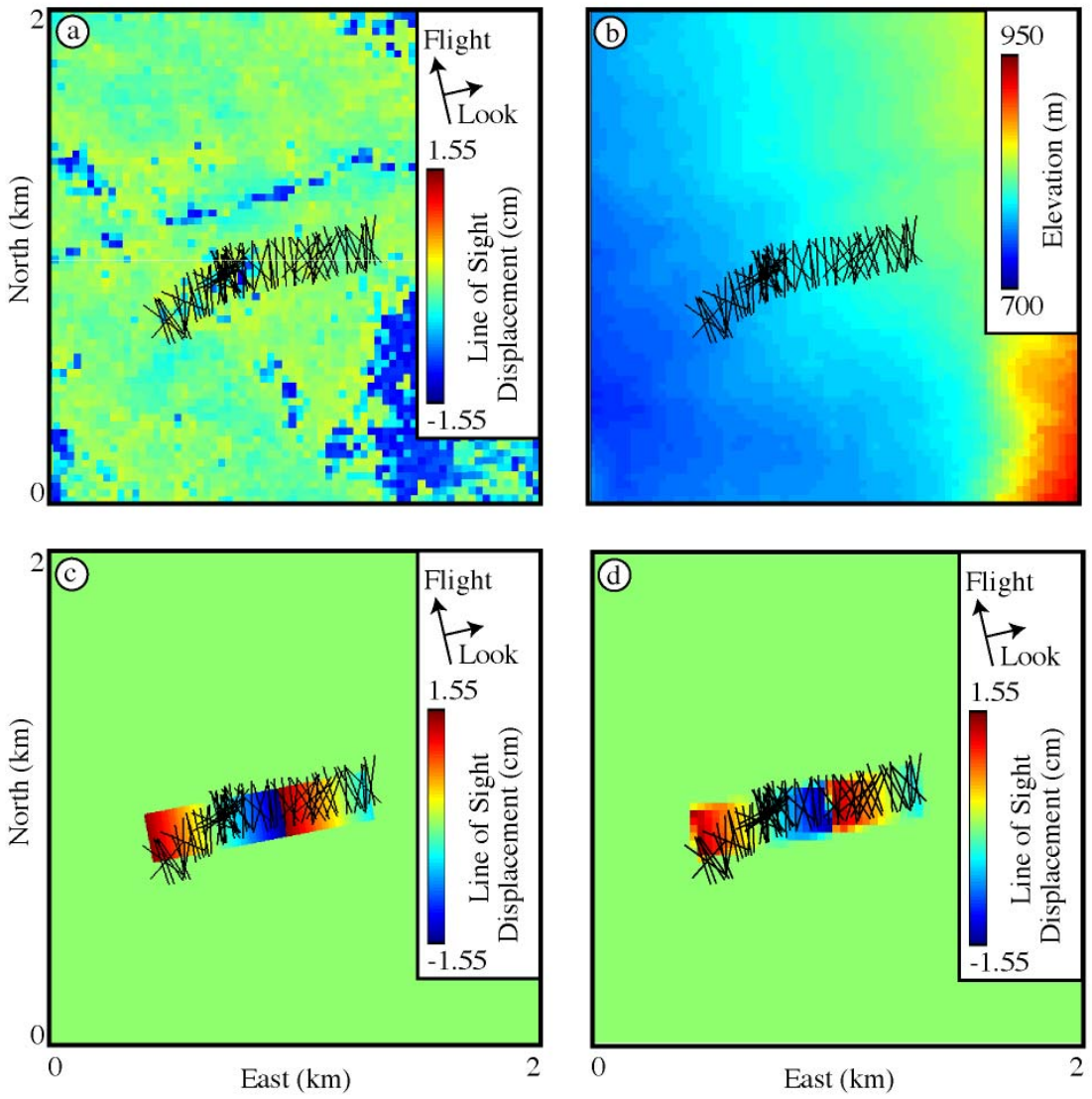

Figure DR8: InSAR-derived line-of-site displacements over the Pisagua site. (a) TerraSAR-X interferogram shown in Figure DR7 zoomed to the area outlined by the black box. The black lines represent measured cracks plotted at a uniform length of 200m. (b) SRTM Digital Elevation Model. Atmospheric noise in the InSAR data, which approximately scales with elevation, is unlikely to significantly contaminate the displacement field across the transect. (c) Predicted line-of-sight displacements across the transect assuming the crack opening field

measurements represent static extension accommodated over the transect, shown at a 1 m resolution. (d) results in (c) resampled to the 30 m resolution of the interferogram in (a).

Figure DR9: Excavated crack profile showing that walls degrade near the surface. This photo is of a crack opening produced during the 2007 M_w 7.7 Tocopilla earthquake. Crack opening in the more competent material at the depth of the scale may better reflect the coseismic strain than the apparent crack opening in the looser sand. Loose eolian sand accumulated in an old surface crack depression has enhanced the new crack opening, which overlies a very fine crack in gypsum fill (lighter material where the scale is located).

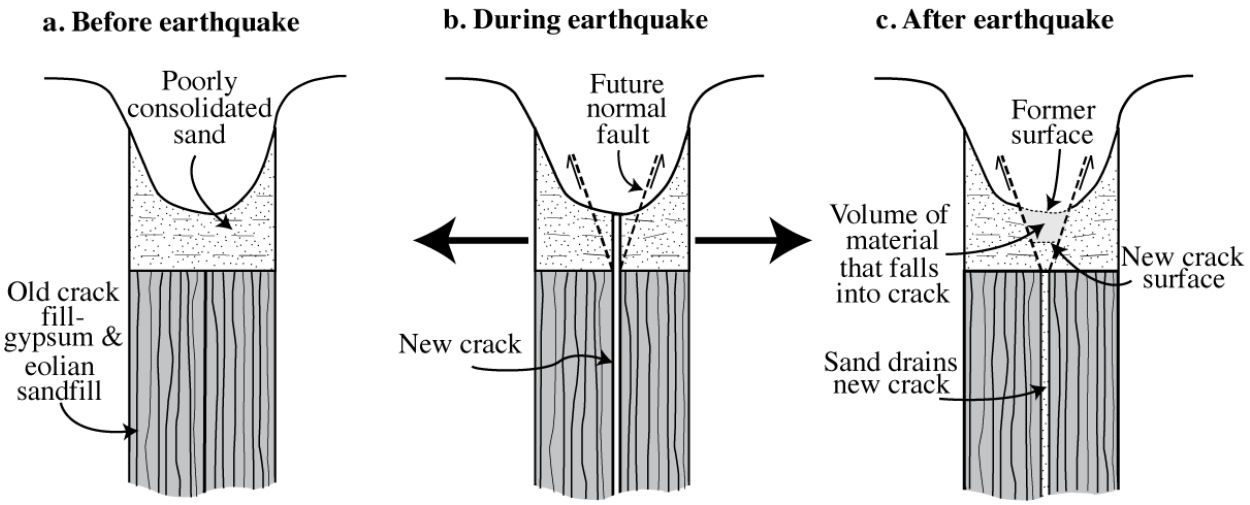

Figure DR10: Schematic illustration of crack opening before, during, and after an earthquake. Where exposes are adequate, cracks can be seen to extend meters to tens of meters into bedrock. The volume of unconsolidated sand that erodes near the surface expression of the crack drains to fill some of the volume created as the pre-existing crack grew during the earthquake. Illustration is not drawn to scale.

Supplementary References:

Allmendinger, R.W., Loveless, J.P., Pritchard, M.E., and Meade, B., 2009, From decades to epochs: Spanning the gap between geodesy and structural geology of active mountain belts: Journal of Structural Geology, v. 31, no. 11, p. 1409–1422, doi: 10.1016/j.jsg.2009.08.008.

Baker, A., Allmendinger, R.W., Owen, L.A., and Rech, J.A., 2013, Permanent deformation caused by subduction earthquakes in northern Chile: Nature Geoscience, v. 6, no. 6, p. 492–496, doi: 10.1038/ngeo1789.

Blewitt, G., 2015, Nevada geodetic laboratory: http://geodesy.unr.edu/billhammond/gpsnetmap/GPSNetMap.html.

Cardozo, N., and Allmendinger, R.W., 2009, SSPX: A program to compute strain from displacement/velocity data: Computers & Geosciences, v. 35, no. 6, p. 1343–1357, doi: 10.1016/j.cageo.2008.05.008.

Farr, T.G., Rosen, P.A., Caro, E., Crippen, R., Duren, R., Hensley, S., Kobrick, M., Paller, M., Rodriguez, E., Roth, L., Seal, D., Shaffer, S., Shimada, J., Umland, J., et al., 2007, The Shuttle Radar Topography Mission: Reviews of Geophysics, v. 45, no. 2, doi: 10.1029/2005RG000183.

Hayes, G.P., Wald, D.J., and Johnson, R.L., 2012, Slab1.0: A three-dimensional model of global subduction zone geometries: Journal of Geophysical Research, v. 117, no. B1, doi: 10.1029/2011JB008524.

Rosen, P.A., Hensley, S., Peltzer, G., and Simons, M., 2004, Updated repeat orbit interferometry package released: Eos, Transactions American Geophysical Union, v. 85, no. 5, p. 47–47, doi: 10.1029/2004EO050004.

Simons, M., Galetzka, J., Genrich, J., Ortega, F., Comte, D., Glass, B., González, G., and Norabuena, E., 2010, Central Andean Tectonic Observatory Geodetic Array:.

Yoon, Y.T., Eineder, M., Yague-Martinez, N., and Montenbruck, O., 2009, TerraSAR-X Precise Trajectory Estimation and Quality Assessment: IEEE Transactions on Geoscience and Remote Sensing, v. 47, no. 6, p. 1859–1868, doi: 10.1109/TGRS.2008.2006983.